Available online at www.sciencedirect.com
SCIENCE DIRECT®
Lithos 75 (2004) 39–54
LITHOS
www.elsevier.com/locate/lithos

# Trace-element partitioning in olivine: modelling of a complete data set from a synthetic hydrous basanite melt

Alberto Zanetti[a,*], Massimo Tiepolo[a], Roberta Oberti[a], Riccardo Vannucci[a,b]

[a] CNR-IGG, Sezione di Pavia, via Ferrata 1, I-27100 Pavia, Italy
[b] Dipartimento di Scienze della Terra, Università di Pavia, via Ferrata 1, I-27100 Pavia, Italy

Received 3 February 2003; received in revised form 9 October 2003; accepted 18 December 2003

Available online 15 April 2004

**Abstract**

Olivine/liquid partition coefficients for most trace elements relevant in petrogenetic studies are provided for a hydrous basanite melt equilibrated at 1.4 GPa and 1055 °C. The partitioning results determined by a combination of EMP and SIMS analyses are discussed in terms of available crystal-chemical mechanisms and crystal-structure control. The critical evaluation of this data set and of those reported in the literature, in the frame of the present lattice-strain model, provides useful suggestions for future studies designed to clarify incorporation mechanisms and site preference in olivine. A further useful suggestion is that the measured $^{Ol/L}D$ values for Li, Mg and Sc allow a straightforward but reliable estimate of the $D_0$ for 1+, 2+ and 3+ cations, respectively. The assessment of $D_0$ for $^{VI}HFSE^{4+}$ is probably biased by their partitioning between the T and M sites. Anyway, it can be reasonably assumed to be close to $^{Ol/L}D_{Zr}$.


*Keywords:* Partition coefficients; Olivine; Hydrous basanite; Trace elements; SIMS analysis

## 1. Introduction

The increasing availability of microanalytical techniques, such as secondary ion mass spectrometry (SIMS) and laser ablation-inductively coupled plasma-mass spectrometry (LA-ICP-MS), has made trace-element analysis of synthetic minerals and glasses easier.

The impressive number of papers concerning solid/liquid trace-element partitioning has also stimulated modelling of the energetic parameters controlling the incorporation processes. The dependence of trace-element partitioning on the physical properties of the available sites in each mineral structure has been rationalised in terms of the relaxation energy (mechanical strain) related to: (i) the difference between the ionic radius of the substituent cations and the optimum radius of the relevant site ($r_0$) and (ii) the rigidity of the lattice around the site, as expressed by its elastic modulus. The principles of this approach have been first established by Nagasawa (1966) and Brice (1975) and have been successfully developed and applied to experimental data by Beattie (1994) and Blundy and Wood (1994). This approach is capable of reproducing in a quite reliable way the physical and energetic properties of different mineral lattice sites (e.g. Wood and Blundy, 1997). However, the effects of structural

* Corresponding author. Tel.: +39-0382-505876; fax: +39-0382-505887.
*E-mail address:* zanetti@crystal.unipv.it (A. Zanetti).

0024-4937/$ - see front matter © 2004 Elsevier B.V. All rights reserved.
doi:10.1016/j.lithos.2003.12.022

constraints are still a matter of debate. Bottazzi et al. (1999), Tiepolo et al. (2000a) and Oberti et al. (2000) investigated trace-element partitioning in various amphibole compositions and found different incorporation mechanisms for REE and HFSE as a function of the actual site dimensions. Van Westrenen et al. (2000) made atomistic simulation of trace-element incorporation in garnets and concluded that, albeit "variations in $r_0$ and the Young's modulus ($E$) result from variations in crystal chemistry", the "absolute values of these parameters can be influenced by the presence and structure of the coexisting melt", so that "quantitative relations between $r_0$, $E$ and crystal chemistry cannot be predicted from crystal-structural data alone". Further atomistic simulation of the pyrope-grossular join, however, brought Van Westrenen et al. (2003) to recognise the importance of the local cation environment, especially of third neighbour interactions, in determining incorporation and site preference in solid solutions.

We provide in this paper a set of olivine/melt partition coefficients ($^{Ol/L}D$) for 24 trace elements [light lithophile elements (LLE), high field strength elements (HFSE), rare earths (REE) and large ion lithophile elements (LILE)] which has been determined by SIMS + EMPA analysis of olivine/melt pairs synthesised at $T$, $P$, $X$ and $f(O_2)$ conditions relevant for upper-mantle studies. Despite their importance in the reconstruction of geochemical and cosmochemical evolution, few data are available on the trace-element partitioning between olivine and anhydrous basaltic melts (McKay, 1986; Colson et al., 1988; Beattie, 1994; Kelemen et al., 1990, 1993; Kennedy et al., 1993; Suzuki and Akaogi, 1995; Taura et al., 1998; Canil and Fedortchouk, 2001; Salters et al., 2002; McDade et al., 2003), whereas no data are available for alkali-rich hydrous systems. Also, the calculated $r_0$ for divalent (0.58–0.81 Å; Beattie, 1994; Purton et al., 2000; Blundy and Wood, 2003a) and trivalent cations (0.58–0.73 Å; Beattie, 1994; Blundy and Wood, 2003a) are highly variable and often very different from those expected on the basis of the aggregate octahedral cation–oxygen distances ($\langle\langle M-O \rangle\rangle$) (see the compilation of M distances in Brown, 1980). Thus, our olivine-melt partitioning data will be discussed in the frame of the lattice-site elastic strain theory in order to place further constraints on the relationship occurring between trace-element partitioning and physical properties of the structural sites.

## 2. The crystal chemistry of olivine

The structure of olivine is rather simple, and its accurate modelling as a function of composition has been made available based on systematic crystal-chemical studies (Della Giusta et al., 1990; Rinaldi et al., 2000).

The olivine structure is built up by one tetrahedral site (occupied by Si) and two independent octahedral sites, M1 and M2, and is characterised by extensive edge-sharing between the polyhedra. This latter feature causes significant distortion due to cation–cation repulsion across shared edges and is thus likely to affect the crystal-chemical behaviour of major and trace elements. The (smaller) M1 octahedron shares 6 out of its 12 edges: 2 with two other M1 octahedra, 2 with two M2 octahedra and 2 with two T tetrahedra. The (larger) M2 octahedron shares only three edges: two with two M1 octahedra and one with a tetrahedron. As a consequence, the tetrahedron shares three out of its six edges.

The crystal chemistry of natural olivines is characterised by extensive solid solution between divalent cations; conversely, monovalent, trivalent and tetravalent cations are always below or close to the EMP detection limits, at least in terrestrial samples. Nearly complete $^{M2}Fe^{3+}\,^{M1}\square^{M1,2}Fe^{2+}_{-2}$ exchange has also been reported, but occurs via a strictly ordered pattern (Janney and Banfield, 1998; Dyar et al., 1998). Olivine with divalent (Be) and pentavalent (P, As) tetrahedral cations as major constituents have been synthesised (see Brown, 1980 and references therein) but are unlikely to occur in nature; in their case, electroneutrality is obtained by the presence of trivalent and monovalent octahedral substituents, respectively. Several mechanisms have been proposed to explain the incorporation of high-charge trace-element substituents in naturally occurring olivine, e.g. the presence of divalent and trivalent cations in the tetrahedron (Beattie, 1994) or of vacancies and monovalent cations in the octahedra (Colson et al., 1989). Purton et al. (1997) calculated solution energies in forsterite and diopside and concluded that the lowest energy pairing in forsterite is $^{M2}R^{3+}/^{M1}Li^{+}$. Taura et al. (1998) showed that the $^{M}Al^{3+}\,^{M}(Li,\,Na)^{1+}\,^{M}Mg^{2+}_{-2}$ exchange becomes more important with increasing pressure.

Studies on cation ordering in olivine have been mainly devoted to the characterisation of the behaviour

of divalent constituents; in particular, they focused on the intracrystalline $Mg-Fe^{2+}$ exchange due to its relevance for geothermometry and for the calculation of the cooling rates of terrestrial rocks and of meteorites. The pattern of $Mg-Fe^{2+}$ ordering in olivine is complex, as $Fe^{2+}$ has a slight preference for the smaller M1 site at $T<880$ °C and a preference for the larger M2 site at higher $T$ (Rinaldi et al., 2000; Redfern et al., 2000 and references therein) due to the increased crystal field stabilisation energy (CFSE) when $Fe^{2+}$ occupies the smaller and less distorted M1 site; this pattern is further complicated by the effect of $f(O_2)$ (Ottonello et al., 1990; Chakraborty, 1997).

## 3. Experimental procedures

### 3.1. Synthesis

The experimental run of this work (T3-1055) belongs to an experimental project aimed to constrain the crystal-chemical control on amphibole/liquid trace-element partitioning and represents a high-temperature trial in which no amphibole crystallisation occurred. All details on synthesis procedure may be found in Tiepolo et al. (2000b). Syntheses were done with a piston cylinder apparatus at $T_{eq}=1055$ °C, $P=1.4$ GPa and starting from a hydrous oxide mixture reproducing the composition of the natural basanite sample WR13-141 from the Mt. Melbourne Volcanic Field (Victoria Land, Antarctica; Worner et al., 1989). The starting mixture has been doped with the following trace elements and nominal concentrations: 35 ppm Li and Be; 70 ppm B, Sr, Y, Zr, La, Ce and Nd; 140 ppm Cr, Nb, Sm and Co; 210 ppm Eu and Gd; 350 ppm Sc and V; 350 ppm Dy, Er and Yb; 700 ppm Hf and Ta. A graphite-lined Pt capsule was used to maintain the oxygen fugacity at the CCO buffer (corresponding to $\sim$ QFM $-2$ at the $P-T$ condition of the T3-1055 run). This experiment is the first test of the trace-element partitioning between olivine and hydrous melt. Run products are olivine (5%), clinopyroxene (15%) and glass.

### 3.2. Major and trace-element analysis

The synthetic mineral phases and the glass were analysed for major elements using a JEOL® JXA-840 scanning electron microscope equipped with 3 WDS analysers at the Centro Grandi Strumenti of the University of Pavia. Operating conditions were 20 kV of accelerating voltage, 20 nA of beam current, 20 s of counting time for each signal, 5-μm$^2$ spot area on the minerals, and 400 μm$^2$ of spot area on the glass to prevent the migration of alkalis. Natural minerals were used as standards (Wakefield Diopside for Si, Ca and Mg, Kaersutite Spring for Al, Fe, Ti and K, Roberts Victor Mine Omphacite for Na, Ilmen Mts. Ilmenite for Mn and Tiebaghi Mine Chromite for Cr). Data reduction was performed by means of the TASK procedure and using the ZAF correction matrix. The results are reported in Table 1. Precision and accuracy have been estimated on the basis of the standards analysis and resulted better than 3% and 10% for major and minor elements, respectively.

The concentration of trace, volatile and light elements in olivine and glass were obtained using a Cameca® IMS 4f ion microprobe (SIMS) located at CNR-IGG (Pavia). The primary beam consisted of mass filtered $^{16}O^-$ and was focused on spots of 15–20 μm diameter onto the sample surface. Analytical conditions were typically 10-nA beam current and 17-keV total impact energy. The ions sputtered from polished, gold-coated samples were transferred to the mass spectrometer by the 25-μm optics and energy filtered by applying $-100$-V offset voltage, with an energy band width by $\pm 25$ eV. Quantification was carried out by means of Si-normalised working curves obtained from well-characterised natural mineral and glass standards. The details of the analytical procedure are reported by Ottolini et al. (1993) and Bottazzi et al. (1994). The secondary intensities were corrected for the background contribution (typically smaller than 0.002 c/s). The analytical accuracy and precision have been assessed by analysing a series of natural and synthetic standards. In particular, the reliability of Ca, Na, Sc, Cr and Co quantification has been tested on the San Carlos olivine [reference values by Köhler and Brey (1990) and Max-Planck Institute compilation]. The estimated accuracy of our analysis is $\sim$ 10% for all the trace elements with absolute concentration at parts-per-million level and $\sim$ 30% for trace elements at tens of parts-per-billion level. Systematic analytical errors affecting sensitivity factors are virtually eliminated in the partition coefficients.

Table 1
Major element composition (SEM + WDS analysis) of olivine and glass from T3-1055 experimental run and calculated compositional ratios/partition coefficients

| | Olivine | | Glass | | $^{Ol/L}D$ | |
|---|---|---|---|---|---|---|
| | Average[a] | St. dev. | Average[b] | St. dev. | | St. dev. |
| $SiO_2$ (wt.%) | 38.89 | 0.40 | 44.40 | 0.52 | 8.8e−1 | 1e−2 |
| $TiO_2$ | | | 1.71 | 0.05 | | |
| $Al_2O_3$ | 0.099 | 0.028 | 16.26 | 0.06 | 6.1e−3 | 1.7e−3 |
| FeO | 19.43 | 0.55 | 12.09 | (0.31)[c] | 1.6e+0 | 6e−2 |
| $Fe_2O_3$ | | | 0.60 | | | |
| MnO | | | 0.02 | 0.02 | | |
| MgO | 41.02 | 0.59 | 3.28 | 0.12 | 1.3e+1 | 5e−1 |
| CaO | 0.30 | 0.02 | 5.73 | 0.27 | 5.2e−2 | 4e−3 |
| $Na_2O$ | | | 5.58 | 0.18 | | |
| $K_2O$ | | | 2.33 | 0.12 | | |
| Sum oxides | 99.74 | | 91.99 | | | |
| Unit formulae | | | | | | |
| Si (apfu) | 0.999 | | | | | |
| Al | 0.003 | | | | | |
| Mg | 1.571 | | | | | |
| $Fe^{2+}$ | 0.417 | | | | | |
| Ca | 0.008 | | | | | |
| Sum cations | 2.998 | | | | | |
| Mg# (molar) | 79.0 | | 33.0 | | | |
| $^{Ol/L}Kd_{(Fe^{2+}-Mg)}$ | 0.13 | | | | | |

[a] Mean of 30 analyses of olivine core.
[b] Mean of 5 analyses far from the mineral/melt interface.
[c] Standard deviation estimated for $FeO_T$.

### 3.3. Chemical equilibrium and Henry law behaviour

Reliable partition coefficients can be calculated only if chemical equilibrium between mineral and melt is attained and the Henry's law is satisfied. At the adopted doping level, no deviation from the Henry's law behaviour is expected. This assumption has been confirmed by Tiepolo et al. (2000b) on the basis of the systematic analysis of the changes in the $^{Amph/L}D$ values in a large number of experimental syntheses run at different $T$ with the same starting mixture of T3-1055.

In order to check the attainment of chemical equilibrium, textural and compositional features of the run products were investigated. Both olivine and clinopyroxene have euhedral shape and size up to 100 μm. Crystal edges are usually sharp; only few olivine crystals are slightly embayed (< 10-μm depth) (Fig. 1). The glass is optically homogeneous and free from quench crystals. Systematic SEM analysis along line profiles on both olivine and glass confirmed that they are homogeneous, with the only relevant exception of the area (approximately 20 μm wide in total) close to the olivine/glass contact (Fig. 2). In this area, there is a sharp increase in the Fe content of olivine and a significant decrease in both Fe and Mg contents ("olivine component") of the glass; notably, the resorption of the olivine rim affects only the Fe-rich areas. Similar major-element variations had also been observed in previous studies and are regarded as indicator of olivine overgrowth during quenching process (e.g. Taura et al., 1998). As a consequence, only the analyses obtained at the core of the crystal and at more than ~ 30 μm from crystals were considered for calculation of $^{Ol/L}D$'s.

The attainment of chemical equilibrium can also be checked by evaluation of the well-controlled Fe–Mg partitioning between olivine and melt, $^{Ol/L}Kd_{Fe-Mg}$ [defined as $(^{Ol}Fe^{2+}/^{Ol}Mg)/(^{Melt}Fe^{2+}/^{Melt}Mg)$; Roeder and Emslie, 1970]. In most basaltic melts, $^{Ol/L}Kd_{Fe-Mg}$

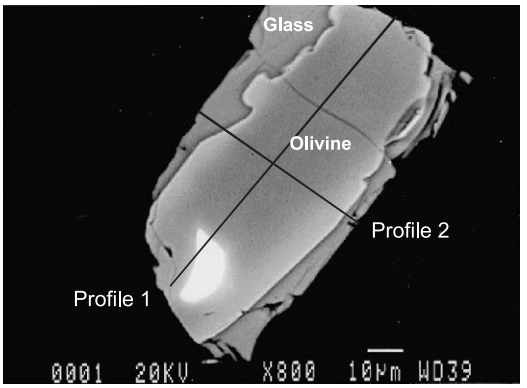


Fig. 1. Scanning electron microscope (SEM) image of an olivine crystal and a portion of the surrounding glass from T3-1055 experimental charge. The tracks of the compositional profiles (by SEM + WDS analysis) documented by Fig. 2 are also reported.

values are around 0.3 (Roeder and Emslie, 1970; Takahashi, 1978; Jones, 1984; Ulmer, 1989; Beattie et al., 1991; Hirschmann and Ghiorso, 1994; Fallon et al., 1997). Nevertheless, several experimental data indicate that the apparent $^{Ol/L}Kd_{Fe-Mg}$ can tend to ~ 0.20 in alkali-rich melts (e.g. Gee and Sack, 1988; Baker et al., 1995, 1996; Draper and Green, 1997; Robinson et al., 1998). Given the large alkali content of the T3-1055 system (a hydrous basanite, according to the classification of Le Maitre et al., 1989), $^{Ol/L}Kd_{Fe-Mg}$ lower than 0.3 could be expected for the olivine/melt pairs. Accordingly, Gee and Sack (1988) obtained $^{Ol/L}Kd_{Fe-Mg} = 0.23 \pm 0.02$ for compositionally similar synthetic systems (i.e. olivine melilitite and nephelinite). The value we obtained in this work for sample T3-1055 is surprisingly low ($0.13 \pm 0.01$) when the $Fe^{3+}/Fe_T$ ratio in the glass (0.05) is estimated according to Kress and Charmichael (1991) for $f(O_2)$ conditions ≅ QFM − 2. Comparable values are documented only in melt inclusions rich in alkali, $Al_2O_3$ and $SiO_2$ found in mantle xenoliths (e.g. Schiano et al., 1992; Hauri et al., 1993; Xu et al., 1996), in which the attainment of the chemical equilibrium is, however, questionable. Nevertheless, the compositional homogeneity of both olivine and glass, as well as the large glass fraction, all suggest equilibrium conditions. A further hypothesis is that the low $^{Ol/L}Kd_{Fe-Mg}$ values are related to some poorly constrained variation of the activity of a major component. Water is most likely excluded because it does not change the $FeO/Fe_2O_3$ in the melt very much and does not enter into the olivine/liquid equilibrium expression (Ghiorso, personal communication). According to Draper and Green (1997), a most viable explanation could be the occurrence in the glass of a larger amount of $Fe_2O_3$ than the estimated one. Melts containing large amounts of alkali metals tend to stabilise $Fe_2O_3$ with respect to FeO, even at low oxygen fugacity (Ghiorso, personal communication). So, it is possible that $Fe_2O_3$ is a substantial fraction or even the dominant form. If this is the case, calculation

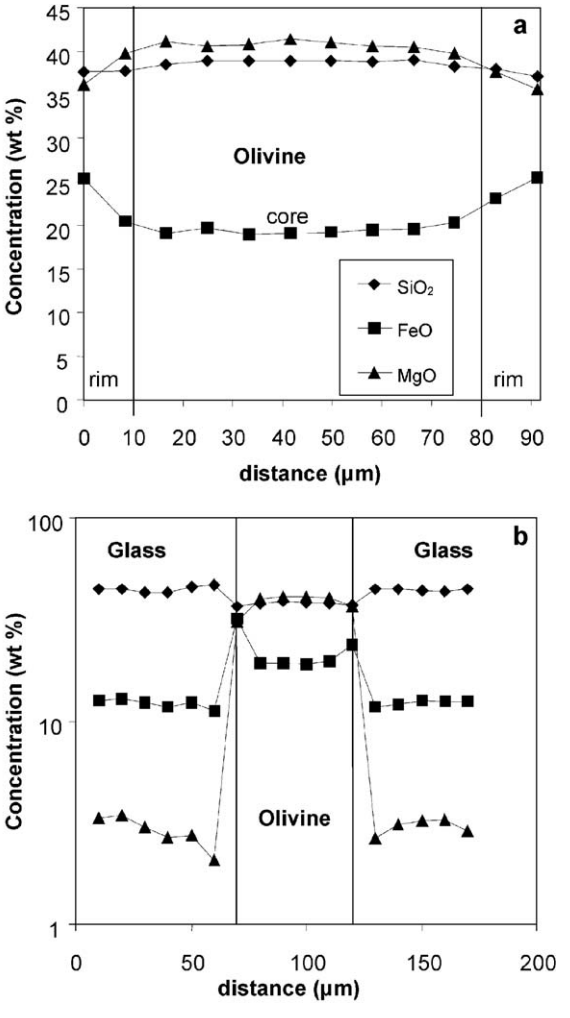


Fig. 2. Compositional profiles across the olivine–melt boundary of T3-1055 shown by Fig. 1. (a) Profile 1; (b) profile 2.

of olivine/liquid Kd based on $FeO_T$ in the liquid would give an unreliable number.

## 4. Partitioning results

The $^{Ol/L}D$ were calculated on the basis of three spots analysed in the core of the olivine crystals and of five spots in the glass. SIMS results, together with the calculated $D$'s, are reported in Table 2. The entire distribution pattern of measured $^{Ol/L}D$ values is shown in Fig. 3. Fig. 4a–d shows the behaviour of the different groups of elements and a comparison with literature data.

Table 2
Trace element composition of olivine and glass from T3-1055 experimental run and calculated partition coefficients

| | Olivine | | Glass | | $^{Ol/L}D$ | |
|---|---|---|---|---|---|---|
| | Average[a] | S. d. | Average[b] | S. d. | Average | S. d. |
| Na (ppm) | 271 | 31 | 41 399 | 1335 | 6.5e−3 | 8e−4 |
| K | 252 | 22 | 19 344 | 996 | 1.3e−2 | 1e−3 |
| Li | 26 | 7 | 116 | 4 | 2.2e−1 | 6e−2 |
| Be | 0.22 | 0.01 | 74 | 0.5 | 2.9e−3 | 2e−4 |
| B | 6.6 | 0.3 | 1141 | 29 | 5.8e−3 | 3e−4 |
| Sc | 194 | 5 | 286 | 13 | 6.8e−1 | 4e−2 |
| Ti | 92 | 13 | 8427 | 170 | 1.1e−2 | 2e−3 |
| V | 51 | 6 | 63 | 4 | 8e−1 | 1e−1 |
| Co | 645 | 7 | 110 | 2 | 5.9e+0 | 1e−1 |
| Sr | 0.231 | 0.006 | 107 | 3 | 2.17e−3 | 9e−5 |
| Y | 0.667 | 0.007 | 177 | 10 | 3.8e−3 | 2e−4 |
| Zr | 0.27 | 0.05 | 60 | 2 | 4.5e−3 | 8e−4 |
| Nb | 0.025 | 0.005 | 145 | 3 | 1.7e−4 | 3e−5 |
| La | 0.011 | 0.008 | 169 | 3 | 6.4e−5 | 5e−5 |
| Ce | 0.014 | 0.003 | 249 | 2 | 5.7e−5 | 1e−5 |
| Nd | 0.031 | 0.012 | 202 | 13 | 1.5e−4 | 6e−5 |
| Sm | 0.086 | 0.029 | 196 | 3 | 4.4e−4 | 2e−4 |
| Eu | 0.181 | 0.052 | 324 | 7 | 5.6e−4 | 2e−4 |
| Gd | 0.32 | 0.01 | 328 | 9 | 9.8e−4 | 5e−5 |
| Dy | 1.40 | 0.35 | 551 | 9 | 2.5e−3 | 6e−4 |
| Er | 3.95 | 0.62 | 435 | 22 | 9.1e−3 | 1e−3 |
| Yb | 15.2 | 0.4 | 270 | 13 | 5.6e−2 | 3e−3 |
| Hf | 0.91 | 0.07 | 243 | 2 | 3.7e−3 | 3e−4 |
| Ta | 0.035 | 0.018 | 1910 | 57 | 1.8e−5 | 9e−6 |
| Cr | 127 | 20 | <10 | | >13 | |
| $Al_2O_3$ (wt.%) | 0.072 | 0.020 | 16.26 | 0.06 | 4.4e−3 | 1.2e−3 |

The concentrations were determined by SIMS, but for Na and K in the glass (SEM+WDS).
[a] Mean of three analyses of olivine core.
[b] Mean of five analyses on glass far from olivine/melt boundary.

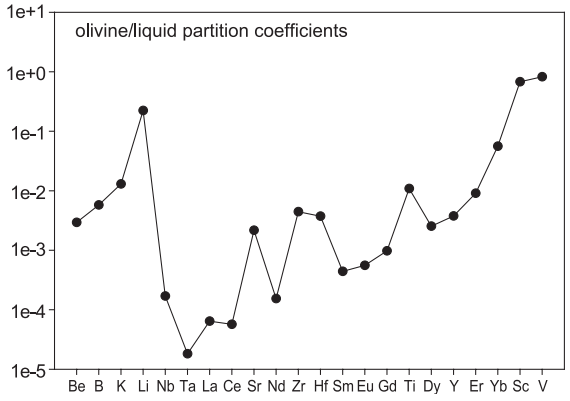


Fig. 3. Olivine/liquid partition coefficients ($^{Ol/L}D$) calculated from the data listed in Table 2 and arranged in the order of ascending compatibility with respect to the mantle peridotites (but Li, which has been arbitrarily placed close to the other LLE).

### 4.1. Light lithophile elements (LLE) and monovalent cations

Very few data on olivine/melt partitioning are available in the literature for monovalent cations (Li, Na and K; hereafter $R^{1+}$) and LLE (Li, Be and B). Reliable SIMS data are reported for Li by Purton et al. (2000), for Li, Be and B by Brenan et al. (1998) and for Li, Na, K, Be and B by Taura et al. (1998). Data on LLE partitioning between olivine and melt are quoted by Brenan et al. (1998). The experiments discussed in Brenan et al. (1998) are those more similar to that of this work because they were performed at $P$–$T$–$X$ conditions relevant to spinel-facies upper-mantle processes (1000–1350 °C and 1.0–1.5 GPa); those discussed by Taura et al. (1998) were done at higher $T$ and $P$ ($T$=1600–2000 °C, $P$=3.0–14.4 GPa).

From our data, the $R^{1+}$ compatibility order in olivine is Li>K>Na, similar to Taura et al. (1998) at 3 GPa. All the experiments done at higher $P$ values gave Li>Na>K. However, $^{Ol/L}D$ for Li and Na from run T3-1055 are 10 and 5 times smaller, respectively, than the minimum values obtained by Taura et al. (1998), consistent with the lower $P$ conditions and to the large pressure dependence of $^{Ol/L}D_{Li,Na}$ reported by the same authors. In fact, the $^{Ol/L}D_{Li}$ value measured for T3-1055 is close to those reported by Brenan et al. (1998). The $^{Ol/L}D_K$ measured for T3-1055 is in the range measured by Taura et al. (1998), which, howev-

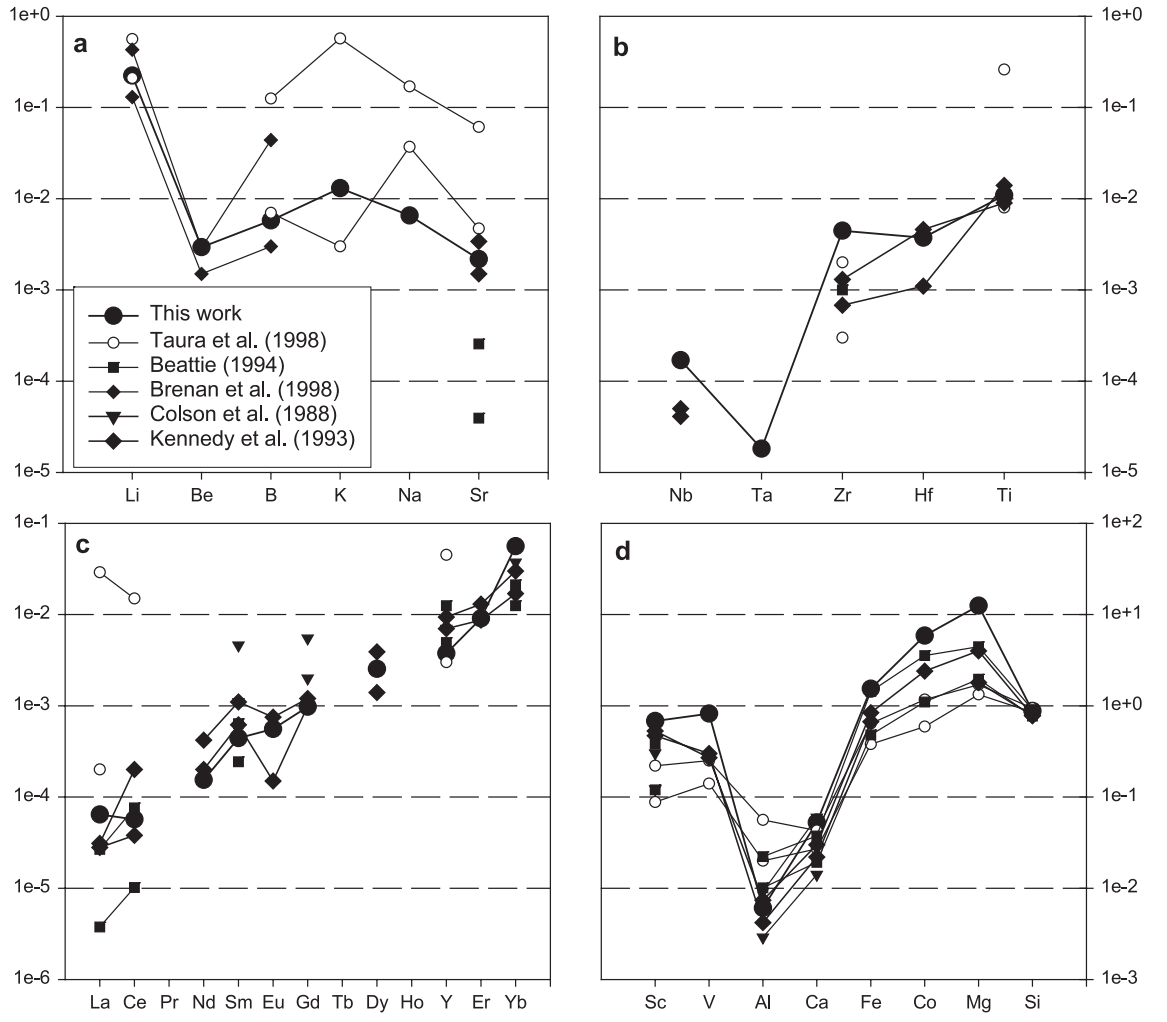


Fig. 4. Comparison between the olivine/liquid partition coefficients determined in this work and literature data. For sake of clarity, only the larger and smaller $^{Ol/L}D$ found by Colson et al. (1989), Beattie (1994), Brenan et al. (1998) and Taura et al. (1998) are shown. The partitioning data from Kennedy et al. (1993) are those from their experimental runs PO 49 and BO 67.

er, does not show any significant correlation with intensive or extensive parameters. Beattie (1994) and Taura et al. (1998) suggested that variable contribution of K from glass contamination can randomly affect the analysis of olivine. On the basis of the composition of the T3-1055 glass, it is expected that if a K excess was brought by glass particles included in or placed on the olivine surface, then the LREE content measured in the olivine should be at parts-per-million level. Given that it is not the case, it can be concluded that, if glass contamination really occurs, it selectively involves K. We also verified that in our SIMS configuration, the residual interference of $^{23}Na^{16}O^{+}$ on $^{39}K^{+}$ contributes $\leq 10$ ppm per 1 $Na_2O$ wt.%. Given that SIMS analysis showed that Na is at the hundreds of parts-per-million level, we can exclude that the K content derives from the $^{23}Na^{16}O^{+}$ contamination.

The relatively large values of $^{Ol/L}D_{Li}$ generally obtained in all the available works suggest that olivine plays a leading role in Li fractionation during upper-mantle processes. Actually, Brenan et al. (1998) showed that at 1.5 GPa, $^{S/L}D_{Li}$ are larger for olivine

than for pyroxene and pargasitic amphibole. Recent investigations on Li partitioning in anhydrous spinel-facies mineral assemblages (Ottolini and McDonough, 1996) also showed that olivine has the highest affinity for Li.

Partition coefficients for B and Be are in the range found by Brenan et al. (1998), with $D_B/D_{Be}$ ratios typically larger than 1. It is noteworthy that the $D_B$ values found by Taura et al. (1998) are systematically larger than our result, suggesting $P$ dependence.

### 4.2. Divalent cations

The $^{Ol/L}D_{Ca}$ measured in run T3-1055 (0.052) is in strict agreement with that predicted by the empirical curve for alkali-rich basaltic systems provided by Libourel (1999).

The $^{Ol/L}D_{Co}$ partition coefficient (5.9) is consistent with prediction according to Hirschmann and Ghiorso (1994) for these MgO content and $T$ conditions.

The $^{Ol/L}D_{Sr}$ value (0.0022) is consistent with those reported by Kennedy et al. (1993) and Taura et al. (1998) ($1.5\times10^{-3}$–$9.1\times10^{-2}$), whereas it is larger than those reported by Beattie (1994) and Purton et al. (2000) ($1\times10^{-4}$–$7\times10^{-5}$). Sr concentrations measured in both olivine and glass from run T3-1055 are well above SIMS detection limits (which are at tens of parts-per-billion level due to the occurrence of residual $^{56}Fe^{16}O_2^+$), and their standard deviations are reasonably small; therefore, the possibility of large analytical errors in the SIMS determinations seems unlikely. Other explanations for the relatively large $^{Ol/L}D_{Sr}$ can be provided and are discussed in a following section.

### 4.3. Trivalent cations

The $^{Ol/L}D_{Al}$ values strongly depend on $P$ and $T$ conditions (Agee and Walker, 1990; Suzuki and Akaogi, 1995; Taura et al., 1998). For run T3-1055, we obtained a value 2 (SIMS data, Table 2) to 3 (EMP + WDS data, Table 1) times larger than that calculated with the $P$–$T$-dependent empirical curve proposed by Agee and Walker (1990) for komatiite and peridotite systems (i.e. 0.0022); this feature implies the presence of residual compositional effects. The dependence of $^{Ol/L}D_{Al}$ from $P$ and $T$ is expected to vary if Al is incorporated into the octahedral or the tetrahedral sites (or partitioned between the two); this feature has not been yet addressed in detail. Taura et al. (1998) calculated the $^{T}$Al and $^{M}$Al contents on the basis of charge-balance considerations involving the entrance of Al, Na and Cr in the olivine structure and showed that the increase in $^{Ol/L}D_{Al}$ at increasing $P$ is basically related to an increase in $^{M}$Al. An application of this procedure to run T3-1055 is discussed in a following section.

$^{Ol/L}D_{REE}$ for run T3-1055 show the typical highly fractionated pattern ($D_{Yb}/D_{La}=87$) and fall in the range defined by the few previous studies reporting $^{Ol/L}D_{REE}$ for more than two elements (McKay, 1986; Colson et al., 1989; Kennedy et al., 1993; Beattie, 1994; Salters et al., 2002; McDade et al., 2003). The partition coefficient measured for Y is in between those for Dy and Er, confirming its strict geochemical affinity with HREE as usually observed in other rock-forming silicates (see, for example, Hart and Dunn, 1993 and Tiepolo et al., 2000b for clinopyroxene and amphibole, respectively).

Few data are available on $^{Ol/L}D$ for V and Sc and have been obtained under very variable $T$–$P$–$X$–$f(O_2)$ conditions; they are in the range 0.004–0.34 and 0.088–0.53, respectively (Kennedy et al., 1993; Suzuki and Akaogi, 1995; Taura et al., 1998; Canil and Fedortchouk, 2001; McDade et al., 2003), therefore far smaller than in run T3-1055 (where $^{Ol/L}D$ for V and Sc is 0.82 and 0.68, respectively).

Notably, the $f(O_2)$ value calculated on the basis of $^{Ol/L}D_V$ for sample T3-1055 according to Canil and Fedortchouk (2001) would suggest very reducing conditions ($\sim$ NNO-6), which is not the case. It can be argued that $f(O_2)$ values predicted on the basis of the absolute $^{Ol/L}D_V$ value will be seriously biased by the changes in the parameters ruling trace-element incorporation in the solid phase (i.e., $D_0$, $r_0$ and $E$). This dependence limits the use of the Canil and Fedortchouk's geobarometer. On the other hand, $D_0$ is the most variable parameter, and thus its effect can be virtually cancelled normalising the $^{Ol/L}D_V$ value to that of an element with only 3+ as possible valence state. Therefore, a new empirical equation was developed by a linear fit of the $D_V/D_{Sc}$ and $f(O_2)$ values reported in Canil and Fedortchouk (2001): $\Delta NNO = -2.46\times\ln(D_V/D_{Sc}) - 2.70$ with $R^2=0.96$. When applied to run T3-1055, it gives NNO $-3.2\pm0.5$, a value consistent with experimental conditions.

### 4.4. Tetravalent and pentavalent cations

$^{Ol/L}D_{Ti}$ and $^{Ol/L}D_{Zr}$ are close to the values considered typical of olivine in spinel-facies mantle assemblages (Kelemen et al., 1990, 1993). For these elements, no systematic variation is evident as a function of $P$–$T$–$X$–$f(O_2)$ conditions. In general, $^{Ol/L}D_{Ti}$ values are restricted in the range (0.01–0.04), whereas $^{Ol/L}D_{Zr}$ values vary by 2 orders of magnitude (in the range of $10^{-3}$–$10^{-5}$: Kelemen et al., 1990 and references therein; Kennedy et al., 1993; Taura et al., 1998; Canil and Fedortchouk, 2001; Salters et al., 2002; McDade et al., 2003). The $D_{Ti}/D_{Zr}$ ratio of the T3-1055 data set is 2.4, being in the range typical of clinopyroxene [which is 1.3–3.3 in the data set by Hart and Dunn (1993), Skulski et al. (1994) and McDade et al. (2003)]. Actually, the $D_{Ti}/D_{Zr}$ values previously reported for olivine in experimental works are higher [between 7 and 21 in Kennedy et al. (1993) and Salters et al. (2002), but 67–375 in McDade et al. (2003)] and more similar to those found for orthopyroxene (most in the range of 2–25: Kennedy et al., 1993; Green et al., 2000; Salters et al., 2002; only one Salters's experiment shows $D_{Ti}/D_{Zr}=66$). In principle, the large variation of $^{Ol/L}D_{Zr}$ might also derive from large analytical errors. On the other hand, the very few literature data available for $^{Ol/L}D_{Hf}$ (which suffers the same analytical problems as $^{Ol/L}D_{Zr}$) define a narrower range (0.001–0.013: Kennedy et al., 1993; Salters et al., 2002; McDade et al., 2003). As a consequence, the $D_{Hf}/D_{Zr}$ values are very variable (0.3–200), whereas they are typically between 1 and 2 in clinopyroxene and amphibole (e.g. Green et al., 2000; Oberti et al., 2000) and in the range 1.0–9.5 in orthopyroxene (Kennedy et al., 1993; Green et al., 2000; Salters et al., 2002; McDade et al., 2003). The $^{Ol/L}D_{Hf}$ measured for T3-1055 is in the range defined by the data of Kennedy et al. (1993) and the $D_{Hf}/D_{Zr}$ value is 0.8.

Experimental data on $D_{Nb}$ have been previously reported only by Kennedy et al. (1993) and McDade et al. (2003) and are in the range of $1.0\times10^{-4}$–$5.5\times10^{-5}$. The $D_{Nb}$ value measured for T3-1055 ($1.7\times10^{-4}$) is coherent with those estimated by Kelemen et al. (1993) on the basis of general considerations on Nb compatibility in upper mantle peridotites. $^{Ol/L}D_{Ta}$ is affected by a large uncertainty (about 50%); however, even at the $2\sigma$ level, it is different and smaller than that of Nb. This finding implies that olivine, together with amphibole (Tiepolo et al., 2000a), may be one of the few mineral phases capable to produce subchondritic Nb/Ta values in liquids during partial melting processes.

## 5. Discussion

### 5.1. Constraints on the substitution mechanisms

The measured concentrations of mono-, di-, tri-, tetra- and pentavalent cations in olivine from run T3-1055 enable us to place some constraints on both the substitution mechanisms ruling local charge balance after incorporation of the high-charge cations at the M sites and the issue of Al partitioning between the M and T sites.

Many previous papers discussed coupled heterovalent exchanges in olivine (Colson et al., 1989; Beattie, 1994; Suzuki and Akaogi, 1995; Purton et al., 1997; Taura et al., 1998). Most of them focused on trivalent cations, and the following crystal-chemical mechanisms were detected: (1) $^{M}R^{3+}\,^{M}\square\,^{M}R^{2+}_{-2}$; (2) $^{T}Al^{3+}\,^{M}R^{3+}\,^{T}Si^{4+}_{-1}\,^{M}R^{2+}_{-1}$; (3) $^{M}R^{1+}\,^{M}R^{3+}\,^{M}R^{2+}_{-2}$. When Fe is the trivalent cation, mechanism (1) should be read as $^{M2}R^{3+}\,^{M1}\square\,^{M1,2}R^{2+}_{-2}$, in agreement with the ordering found in the relevant end member (laihunite) which has been found in meteorites (Janney and Banfield, 1998; Dyar et al., 1998). The few data available for tetra- and pentavalent HFSE cations allow characterisation of their incorporation mechanisms only on a speculative basis. A reasonable hypothesis is that the mechanisms are the same, but the coefficients are varied. Mechanism (1) should be discarded because it would imply too many structural vacancies. In order to verify the role of substitution mechanisms (2) and (3), the concentrations of all the analysed elements were converted in atoms per formula unit and normalised on the basis of 4 oxygen atoms (i.e. $Fe_T=Fe^{2+}$). The bias produced by this assumption will be discussed at the end of this section. Be and B are considered ordered at the T site, and their contribution is of $-0.0001$ valence units (vu). Na and Li contribute $-0.0025$ vu to the octahedron, which could be enhanced to $-0.0035$ if the far less reliable estimate for K was considered. Transition elements (REE, HFSE, Y, Sc and V) contribute with $+0.0019$ vu (of which Ti is responsible for $+0.0006$ vu). The relative importance of mechanisms (2) and (3)

can be assessed under the constrain of electroneutrality and depends on the assumptions on Al and Ti partitioning. Site distribution was thus carried out by considering $Al_2O_3$ analyses by both EMPA and SIMS and assuming Ti ordered either at the T or at the M sites. Be and B were ordered at the T site. Transition elements (but Ti, when it was assumed to order at the T site) were put at the M sites, where they balance the defect of positive charge caused by incorporation of monovalent alkaline elements [mechanism (3)]. The residual defect of positive charge was considered to be provided by an equal amount of $^{M}Al^{3+}$, and the remaining Al was distributed between the T and M sites [mechanism (2)]. Our data suggest that mechanism (3) is dominant; it accounts for 67–75% of the heterovalent substitutions when K is neglected and Ti is ordered at the M sites and up to 89–100% when K is considered and Ti is ordered at the T site. In the first model, 67–63% of the total Al content is ordered at the M sites [mechanisms (2) and (3)], which becomes 73–81% if Ti is located at the T site. In the second model, we obtain the following partitioning: 79–90% $^{VI}$Al when Ti is ordered at M sites and 89–100% $^{VI}$Al when Ti is ordered at the T site. If some $Fe^{3+}$ were present, the percentage of $^{IV}$Al would increase.

The available relative concentrations of Li, Na and K in primitive MORB are 3–6 ppm, 2.5–2.7 wt.% and 0.1 wt.%, respectively (Ryan and Langmuir, 1987; Hofmann, 1988), and in most of OIB basalts are <8 ppm, >2.5 wt.% and >0.9 wt.%, respectively (Ryan and Langmuir, 1987). Therefore, Na will be always the most abundant monovalent cation in the natural magmatic olivines, albeit its distribution coefficient is smaller than that of Li.

### 5.2. Lattice-strain model fit to the experimental data and trace-element incorporation in olivine

Models for trace-element partitioning into olivine are based upon fits of experimentally determined $^{Ol/L}D$ values to equations describing the lattice strain determined by the mismatch between the ionic radii of the trace cations and the size of the relevant site (Beattie, 1994; Purton et al., 2000). The model parameters calculated so far from the fitting of divalent and trivalent cations were in a poor agreement with the structural parameters of olivine. In particular, the optimum ionic radii ($r_0$) modelled by Beattie (1994) (0.58 Å for divalent and trivalent cations) and Purton et al. (2000) (0.63 Å for divalent cations in forsterite) are very small with respect to the realistic estimates of the aggregate ionic radii of the octahedral sites, either done from site populations and tabulated (Shannon, 1976) ionic radii ($r_S$; $^{VI}r_{Mg}=0.72$ Å and $^{VI}r_{Fe}^{2+}=0.78$ Å) or from measured ⟨M–O⟩ mean bond lengths. For instance, $\langle M1-O\rangle = 2.101(1)$ Å and $\langle M2-O\rangle = 2.135(1)$ Å in forsterite (Brown, 1980); therefore, the minimum values of the aggregate ionic radii of the actual site of incorporation ($r^*$), obtained subtracting the $^{IV}O^{2-}$ ionic radius (1.38 Å; Shannon, 1976), are 0.721 and 0.755 Å, respectively. Optimum ionic radii more consistent with the geometric parameters of the olivine octahedra ($r_0^{3+}=0.70–0.73$ Å; $r_0^{2+}=0.78–0.82$ Å) have been only recently determined by Blundy and Wood (2003a), who have refitted to the lattice strain model various sets of olivine/melt partition data reported in literature including both the $^{Ol/L}D$ for Sc and $^{VI}$Al along with those for lanthanides.

The agreement between the structure details and the fitting parameters is crucial to understand whether the incorporation models are correct and to what extent the crystal structure may affect trace-element incorporation. In this section, we report the fitting of the various $^{Ol/L}D$ values obtained for olivine T3-1055 and a critical comparison of the resulting model parameters with the $r_S$ calculated for the M1 and M2 octahedra on the basis of its (core) composition and the expected Mg–$Fe^{2+}$ ordering at 1055 °C. According to the latest model of cation ordering in olivine (Rinaldi et al., 2000), $Fe^{2+}$ should be mostly ordered at the M2 site at the $T$ conditions relevant for sample T3-1055. Therefore, the calculated $r_S$ and $r^*$ for the two independent M sites are $^{M1}r_S=0.73$ Å; $^{M2}r_S=0.74$ Å; $^{M1}r^*=0.730$ Å; $^{M2}r^*=0.767$ Å.

#### 5.2.1. Trivalent cations

Due to their configurations of *d*-electrons, the partitioning behaviour of $V^{3+}$ and $Cr^{3+}$ is affected by crystal-field stabilisation energy (CFSE). The sign of the deformation energy related to this effect ($Q_{CFSE}$) depends on the relative size and the electronegativity of the transition metal with respect to that of the «host» cation (for a discussion, cf. Urusov, 2001 and references therein). At similar electronegativity, $Q_{CFSE}$ is negative when the transition metal is larger than the "host" cation and positive in the other case. Thus, the

entrance of $Cr^{3+}$ and $V^{3+}$ in the $Mg–Fe^{2+}$ olivines ($r_{Cr,V} < r_{Mg,Fe}^{2+}$) implies $Q_{CFSE}>1$ and a stronger preference of these cations for the olivine phase than for the more-distorted environment of the melts (Keppler, 1992). Olivine/liquid partitioning of Cr and V is further complicated by the possible presence of variable amounts of $Cr^{2+}$ (Hanson and Jones, 1998) and $V^{4+}$ (Canil and Fedortchouk, 2001), which increase and decrease, respectively, the total $^{Ol/L}D$ value. Therefore, the trend $D_{Cr} \gg D_V > D_{Sc}$ observed in run T3-1055, as well as in other studies (e.g. Kennedy et al., 1993; Suzuki and Akaogi, 1995; Taura et al., 1998; Canil and Fedortchouk, 2001), derives from positive values of $Q_{CFSE}$ and should not be considered in the fits if the CFSE contribution has not been estimated.

The $D$ values measured for octahedral trivalent cations were plotted as a function of their ionic radii in [6]-fold coordination (Fig. 5). The $D$ values measured for REE with ionic radius larger than Nd deviate progressively from the pseudo-parabolic trend connecting HREE, Sc and Al. $^{Ol/L}D$ values for M-LREE larger than to those for HREE are common in the literature [see, for example, the comparison done by Beattie (1994) and the large variation in $^{Ol/L}D_Y/^{Ol/L}D_{La}$ values shown by the data of Taura et al. (1998)]. Due to their low absolute concentrations in olivines, and thus to the large standard deviation, this behaviour could, in principle, be a consequence of very low amount of glass contamination (<0.01%) and/or of approaching SIMS detection limits (at parts-per-billion level for LREE).

We tentatively fit $^{Ol/L}D$ for trivalent trace elements considering the two independent octahedra, i.e. by accepting two different values for $r_0$ and $E$, and found that this model may account the observed fractionation. However, their concentrations are very low, and thus reliable fits should be based on some a priori assumption on the acceptable $r_0$ and/or $E$ values. The present knowledge on olivine crystal chemistry and on the structural differences of the two octahedral sites can be used to this purpose; however, more experimental work is needed to assess this procedure. In practice, fitting $^{Ol/L}D$ values for REE over the two octahedra would significantly affect only the $E$ values.

When fitting $D$ values of Sc, Y and REE from Yb to Nd, neglecting Eu, the calculated $r_0$, $E$ and $D_0$ are 0.74 Å, 585 GPa and 0.70, respectively (Table 3). Notably, the $^{Ol/L}D_{Al}^{VI}$ value obtained by this fit (0.004)

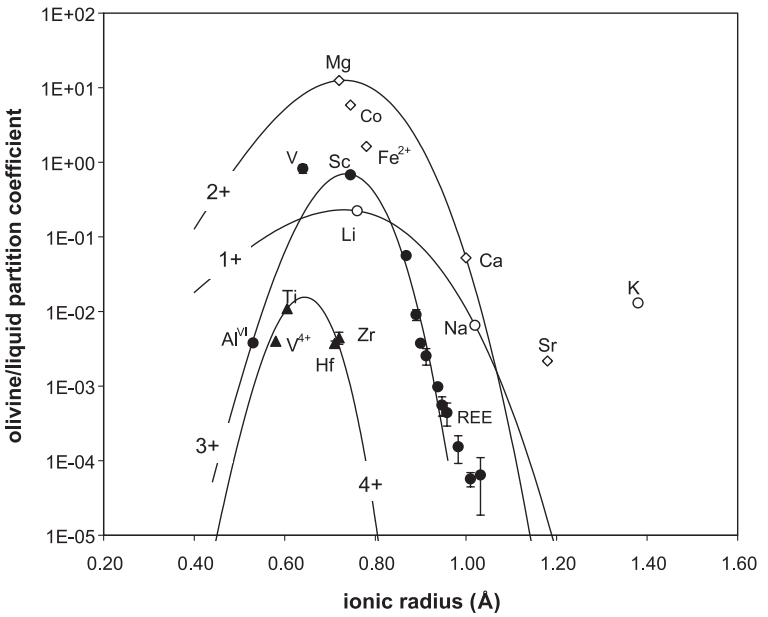


Fig. 5. Olivine/liquid partition coefficients for major and trace element versus cation radii for [6]-fold coordination. The pseudo-parabolic curves represent the fit of the measured $^{Ol/L}D$'s for isovalent elements to the Eq. (2) of Blundy and Wood (1994). The $^{Ol/L}D_{V4+}$ value is taken from the experimental run 129adk1 of Canil and Fedortchouk (2001).

Table 3
Parameters determined by fitting the olivine-melt partitioning data from T3-1055 experimental run to the lattice strain model and considering a [6]-fold octahedral site

| Cations | $r_0$ (Å) | $E$ (GPa) | $D_0$ |
|---|---|---|---|
| Monovalent | [a] | 134 | 0.23 |
| Divalent | [a] | 241 | 12.6 |
| Trivalent | 0.74 | 585 | 0.70 |
| Tetravalent[b] | 0.64 | 1107 | 0.016 |

[a] Optimum radius fixed in the modelling in agreement with $r_S$ (namely, 0.73 Å).

[b] If Ti was ordered at the T site, $r_0$ and $D_0$ are estimated to be ~ 0.73 Å and ~ 0.0045, respectively.

is very close to that estimated on the basis of the reasoning discussed above to determine site populations; this agreement gives more strength to both procedures. The values obtained for $r_0$ (0.74), $r_S$ (0.73) and $r^*$ [(0.734 + 0.764)/2 = 0.749 Å] are in good agreement, suggesting that incorporation of the trivalent cations is strongly controlled by the olivine structure. The ionic radius of Sc is very close to $r_S$ and $r^*$, and therefore the knowledge of $^{Ol/L}D_{Sc}$ provides a straightforward and reliable estimate of the $D_0^{3+}$.

The $E$ value estimated on the basis of the behaviour of trivalent cations for the aggregate octahedral sites of olivine T3-1055 (585 GPa) is in strict agreement with that determined for $D_{HREE}$ at the large octahedral M2 site in richterite (528 GPa; Bottazzi et al., 1999). On the other hand, it is significantly smaller than that (1635 GPa) reported by Hill et al. (2000) and larger than the range (21–46 GPa) determined by Canil and Fedortchouk (2001), which, however, are both affected by the lack of correction for CFSE on $D_V$ and $D_{Cr}$. The very small $r_0^{3+}$ calculated by Beattie (1994) and Hill et al. (2000), as well as the extreme variability of those found by Canil and Fedortchouk (2001), can be reasonably ascribed to the same effect. The $E$ for $R^{3+}$ of olivine T3-1055 is large when compared with those usually reported in literature for [8]-fold coordinated trivalent cations in clinopyroxene and orthopyroxene (260–390 GPa; e.g. Hill et al., 2000; Green et al., 2000). $E$ values more similar to that of this study have been found at the dodecahedral X site in garnet (450–720 GPa; Green et al., 2000).

### 5.2.2. Divalent cations

Large deviations from the bell-shaped trend expected from the lattice-strain theory are present also for octahedral divalent cations. Again, deviations for $Fe^{2+}$ and $Co^{2+}$ can be explained by both the significant CFSE contribution and the difficult evaluation of the valence state especially in the melt. When excluding Fe and Co, no reasonable fit can be obtained which takes into account $^{Ol/L}D$ for Mg, Ca and Sr. This feature is not a peculiarity of our data set, but it is present in all the recent high-quality $^{Ol/L}D$ sets obtained using ion microprobe (e.g. Kennedy et al., 1993; Taura et al., 1998. The presence of preferential order between the M1 and M2 sites for some divalent cation could also affect lattice-strain model; however, the difference between the two $r_S$ is small, and a two-site fit is impossible with the available data. The fitting procedure was also done by using only the $^{Ol/L}D$ for Mg and Ca (Fig. 5). This procedure requires that one out of the three fitting parameters ($r_0$, $D_0$ and $E$) is constrained; we decided to fix $r_0^{2+}$ because sound structural information are available. It is also known that $r_0^{2+}$ should be smaller than $r_0^{3+}$. Blundy and Wood (2003a) showed that in olivine, $^{VI}r_0^{2+}$ is 0.078 Å larger than the associated $^{VI}r_0^{3+}$. In analogy with these results, a $^{VI}r_0^{2+}$ value of 0.815 Å should be used for olivine T3-1055. This value is, however, significantly larger than both $r_S$ and $r^*$ calculated on the basis of the composition and even larger than the $r^*$ estimated for the M1 and M2 sites of fayalite (0.778 and 0.798 Å for M1 and M2, respectively). Therefore, we decided to perform the fit using a $r_0 = r_S$ value of 0.73 Å; in this way, the calculated $E$ value is 241 GPa.

Hazen and Finger (1979) examined a series of oxides and obtained the relation $Kd^3/Z = 750 \pm 20$ GPa Å$^3$, where $K$ is the bulk modulus, $Z$ is the cation charge and $d$ is the cation–oxygen distance; Wood and Blundy (1997) found that $E \sim 1.5K$. $E$ values of 227 and 240 GPa can be calculated starting from the observed ⟨M–O⟩ distances for the M1 and the M2 site, respectively. These $E$ values are consistent with those (210 and 195 GPa) obtained from the bulk moduli measured by Kudoh and Takéuchi (1985) on forsterite. On the contrary, Purton et al. (2000) calculated a very small $E$ value (143 GPa) from their $^{Ol/L}D$ data. However, their results are biased by the use of the $^{Ol/L}D$ measured for major elements with variable valence (i.e. 2+ and 3+) and/or $Q_{CFSE}$ (e.g. Ni), which would explain also the small calculated $r_0^{2+}$ (0.63 Å). Further investigations are needed to better constrain

the relation between the measured $K$ values and the modelled $E$ values in olivine.

Similarly to the previous discussion done for LREE, the largest divalent cation (Sr) falls well away from the parabolic trend connecting Mg and Ca. This feature gives further strength to the idea that small and large isovalent trace elements may have distinct ordering patterns, and that their budget can be precisely accounted for only when considering that they can partition between the two independent octahedra or assume a distinct coordination. This issue has been discussed in detail in the case of amphiboles by Bottazzi et al. (1999). Further experiments should be specifically designed to verify this hypothesis in the case of olivine.

#### 5.2.3. Monovalent cations

In a similar way, a fit of $^{Ol/L}D$ measured for monovalent cations was attempted using only Li and Na and assuming $r_0 = r_S$. Given that $^{VI}r_{Li} = 0.74$ Å (Shannon, 1976), a reliable estimate of $D_0^{1+}$ should be straightforwardly obtained from $^{Ol/L}D_{Li}$. The $E$ value calculated in this way (134 GPa) is very close to that estimated (114–120 GPa) by using the equation of Hazen and Finger (1979).

#### 5.2.4. Tetravalent cations

The estimate of the model parameters ruling the incorporation of $HFSE^{4+}$ in the olivine structure is seriously biased by the lack of information on Ti site preference.

On the basis of the relationships occurring among the $^{Ol/L}D$ and the absolute concentration of Si and $HFSE^{4+}$, Kennedy et al. (1993) and Canil and Fedortchouk (2001) proposed that Ti is incorporated into the T site in olivine. The tetrahedral site in olivine is larger and more distorted than many tetrahedra occurring in other families of rock-forming minerals. It can be compared only to the T2 site in amphibole, the site in which tetrahedral Ti has been shown to order in richterite (Oberti et al., 1992); in that case, the ⟨T2–O⟩ distance is ≥1.635 Å, and the angular variance is around 35°, to be compared with 1.637 Å and 44° measured on the refined olivine crystal of this work (unpublished data). The observed HFSE fractionation ($D_{Hf}/D_{Zr} < 1$ and $D_{Ti}/D_{Zr} > 1$) is also consistent with a different site preference for Ti and Zr(Hf). On the other hand, no sound information is available, and highly variable $D_{Ti}/D_{Zr}$ and $D_{Hf}/D_{Zr}$ values have been published. This latter feature in particular may suggest that HFSE can assume distinct pattern of order as a function of the different experimental $T$–$P$–$X$–$f(O_2)$ conditions. The presence of $Ti^{3+}$ should be discarded at the $f(O_2)$ conditions of the present work.

Therefore, we fitted the measured values of $^{Ol/L}D_{HFSE^{4+}}$ considering either an octahedral or a tetrahedral site preference for $Ti^{4+}$. In the former case, we obtained $r_0^{4+} = 0.64$ Å, $E = 1110$ GPa and $D_0 = 0.016$ (Fig. 5), where $r_0$ is comparable with those obtained by fitting $D_{HFSE^{4+}}$ data for clinopyroxenes (e.g. Hill et al., 2000 and references therein) and amphiboles (when Ti is correctly partitioned among the various M and T sites as explained by Oberti et al., 2000). Notably, the value of $^{Ol/L}D_V^{4+}$ (0.006) predicted by this fit is very close to that measured (0.004) by Canil and Fedortchouk (2001) in an experiment performed in air, thus suggesting that most, if not all, V had been oxidised to 4+.

If Ti is considered ordered at T site, the calculated $r_0$ value for $^{VI}HFSE^{4+}$ is 0.73–0.74 Å, still compatible with that calculated for 3+ cations. In this case, the $D_0$ value would be now close to $D_{Zr}$.

## 6. Evaluation of the results

The reliability of the above conclusions and data treatment can be evaluated by careful control of the dependence of the $E$ and $D_0$ parameters on cation charge. Based on the results of lattice-strain modelling for clinopyroxene/melt partitioning data, Hill et al. (2000) confirmed a linear trend for the M2 site and proposed a logarithmic relation for the M1 site. Blundy and Wood (2003b) showed that the apparent $E$ value estimated by fitting experimental solid–melt partitioning data of different silicates to the lattice strain model agreed well with those of oxides at values of $Z_c/d^3$ lower than 0.3 (which are typical of trivalent cations in [6]-fold coordination), whereas it is considerably stiffer at higher $Z_c/d^3$ values. Our data confirm this trend. In particular, the increase of the apparent $E$ value with $Z_c/d^3$ is exponential, whether or not the less reliable $E$ value calculated for tetravalent cations is considered.

The strain-compensated optimum partition coefficients ($D_0$) estimated in this work define the following

trend: $D_0^{2+} > D_0^{3+} > D_0^{1+} \gg D_0^{4+}$. Comparison of our data with those of Taura et al. (1998) indicates that this trend is consistent with the low $P$ conditions of the experiment. Wood and Blundy (2001) and Blundy and Wood (2003b) proposed a simple model to predict the influence of cation charge on $D_0$, which is based on the observation of their parabolic dependence. However, the $D_0$ values calculated from run T3-1055 do not strictly lie on a parabola, similarly to those calculated in Kennedy et al. (1993) and Taura et al. (1998). This feature suggests that other constraints may also play a relevant role or/and that some model assumptions might be modified.

## 7. Concluding remarks

This study confirms that the size of the octahedral sites exerts a strict control on the partitioning of mono-, di- and trivalent elements between olivine and liquid. Macroscopic properties of the olivine structure should thus be taken into more account as reliable constraints for geochemical modelling done either by lattice-strain formulations or atomistic computer simulations. Investigations of trace-element behaviour in amphiboles brought us to the conclusion that the actual dimension of each site, as well as their relations, can strongly affect site preference and incorporation. In particular, Bottazzi et al. (1999) found that the $r_0^{3+}$ values calculated for [6]- and [8]-fold coordinated sites coincide with the average ionic radius ($r^*$) of the actual site of incorporation. Oberti et al. (2000) found that the contribution to mineral/liquid $D$ for elements that can partition themselves between different sites can and should be separated. Tiepolo et al. (2000a) demonstrated that $Nb^{5+}$ and $Ta^{5+}$ show a strong preference for a coordination with smaller M–O distances and higher distortion such as that of $Ti^{4+}$ in the M1. The preference for highly distorted coordination shown by HFSE, and its implication on the covalent nature of the chemical bonding, can in some way influence the energetics involving their incorporation in the minerals. We suggest that accurate structure refinements and reliable site populations for major elements are absolutely required to unravel the complex mechanisms of trace-element incorporation in minerals and to provide realistic estimates of $r_0$ for mono-, di- and trivalent cations in predictive models of mineral/melt partitioning based on elastic-strain theory.

This work also provides some useful rules of thumb. The measured $^{Ol/L}D$ values for Li, Mg and Sc allow a straightforward but reliable estimate of the $D_0$ for 1+, 2+ and 3+ cations, respectively. Albeit biased by some disorder between the T and M sites, the $D_0$ value for $^{VI}HFSE^{4+}$ can be reasonably assumed to be close to $^{Ol/L}D_{Zr}$.

## Acknowledgements

Syntheses were done at the Mineralogisch-Petrologisches Institut of Göttingen under the supervision of Steve Foley, who is gratefully thanked for his help to MT. M.S. Ghiorso and A. Boudreau are greatly thanked for their comments and suggestions about the assessment of the olivine/melt equilibrium. Jon Blundy and Trevor Green are particularly thanked for their constructive reviews. This research was funded by Ministero dell'Istruzione, dell'Università e della Ricerca (PRIN 2002 Project «Geo-crystal-chemistry of trace elements») and by Consiglio Nazionale delle Ricerche.

## References

Agee, C.B., Walker, D., 1990. Aluminium partitioning between olivine and ultrabasic silicate liquid to 6 GPa. Contrib. Mineral. Petrol. 105, 243–254.

Baker, M.B., Hirschmann, M.M., Ghiorso, M.S., Stolper, E.M., 1995. Compositions of near-solidus peridotite melts from experiments and thermodynamic calculations. Nature 375, 308–311.

Baker, M.B., Hirschmann, M.M., Wasylenki, L.E., Stolper, E.M., Ghiorso, M.S., 1996. Quest for low-degree mantle melts (scientific correspondence). Nature 381, 286.

Beattie, P., 1994. Systematics and energetics of trace-element partitioning between olivine and silicate melts: implications for the nature of mineral/melt partitioning. Chem. Geol. 117, 57–71.

Beattie, P., Ford, C., Russell, D., 1991. Partition coefficients for olivine–melt and orthopyroxene–melt systems. Contrib. Mineral. Petrol. 109, 212–234.

Blundy, J.D., Wood, B.J., 1994. Prediction of crystal-melt partition coefficients from elastic moduli. Nature 372, 452–454.

Blundy, J.D., Wood, B.J., 2003a. Mineral-melt partitioning of uranium, thorium and their daughters. In: Bourdon, B., et al., (Eds.), Uranium-Series Geochemistry. Rev. Mineral. Geochem. 52, pp. 59–118.

Blundy, J.D., Wood, B.J., 2003b. Partitioning of trace elements between crystals and melts. Earth Planet. Sci. Lett. 210, 383–397.

Bottazzi, P., Ottolini, L., Vannucci, R., Zanetti, A., 1994. An accurate procedure for the quantification of rare earth elements in silicates. In: Benninghoven, A., Nihei, Y., Shimizu, R., Werner, H.W. (Eds.), Secondary Ion Mass Spectrometry, SIMS IX Proceedings. Wiley, Chichester, pp. 927–930.

Bottazzi, P., Tiepolo, M., Vannucci, R., Zanetti, A., Brumm, R.C., Foley, S.F., Oberti, R., 1999. Distinct site preference for heavy and light REE in amphibole and the prediction of $^{Amph/L}D_{REE}$. Contrib. Mineral. Petrol. 137, 36–45.

Brenan, J.M., Neroda, E., Lundstrom, C.C., Shaw, H.F., Ryerson, F.J., Phinney, D.L., 1998. Behaviour of boron, beryllium, and lithium during melting and crystallisation: constraints from mineral-melt partitioning experiments. Geochim. Cosmochim. Acta 62, 2129–2141.

Brice, J.C., 1975. Some thermodynamic aspects of the growth of strained crystals. J. Cryst. Growth 28, 249–253.

Brown, G.E., 1980. Olivine and silicate spinels. In: Ribbe, P.H. (Ed.), Orthosilicates. Rev. Mineral., vol. 5, pp. 275–381.

Canil, D., Fedortchouk, Y., 2001. Olivine–liquid partitioning of vanadium and other trace elements, with applications to modern and ancient picrites. Can. Mineral. 39s, 319–330.

Chakraborty, S., 1997. Rates and mechanisms of Fe–Mg interdiffusion in olivine. J. Geophys. Res. 78, 6852–6862.

Colson, R.O., McKay, G.A., Taylor, L.A., 1988. Temperature and composition dependencies of trace element partitioning. Olivine/melt and low-Ca pyroxene/melt. Geochim. Cosmochim. Acta 52, 539–553.

Colson, R.O., McKay, G.A., Taylor, L.A., 1989. Charge balancing of trivalent trace elements in olivine and low-Ca pyroxene: a test using experimental partitioning data. Geochim. Cosmochim. Acta 53, 643–648.

Della Giusta, A., Ottonello, G., Secco, L., 1990. Precision estimates of interatomic distances using site occupancies, ionisation potentials and polarizability in *Pbnm* silicate olivines. Acta Cryst. B46, 160–165.

Draper, D.S., Green, T.H., 1997. $P–T$ phase relations of silicic, alkaline, aluminous mantle–xenolith glasses under anhydrous and C–O–H fluid-saturated conditions. J. Petrol. 38, 1187–1224.

Dyar, M.D., Delaney, J.S., Sutton, S.R., Schaefer, M.W., 1998. $Fe^{3+}$ distribution in oxidized olivine: a synchrotron micro-XANES study. Am. Mineral. 83, 1361–1365.

Fallon, T.J., Green, D.H., O'Neill, H.St.C., Hibberson, W.O., 1997. Experimental tests of low degree peridotite partial melt compositions: implications for the nature of anhydrous near solidus peridotite melts at 1 GPa. Earth Planet. Sci. Lett. 152, 149–162.

Gee, L.L., Sack, R.O., 1988. Experimental petrology of melilite nephelinites. J. Petrol. 29, 1233–1255.

Green, T.H., Blundy, J.D., Adam, J., Yaxley, G.M., 2000. SIMS determination of trace element partition coefficients between garnet, clinopyroxene and hydrous basaltic liquids at 2–7.5 GPa and 1080–1200 °C. Lithos 53, 165–187.

Hanson, B., Jones, J.H., 1998. The systematics of $Cr^{3+}$ and $Cr^{2+}$ partitioning between olivine and liquid in the presence of spinel. Am. Mineral. 83, 669–684.

Hart, S.R., Dunn, T., 1993. Experimental cpx/melt partitioning of 24 trace elements. Contrib. Mineral. Petrol. 113, 1–8.

Hauri, E.H., Shimizu, N., Dieu, J.J., Hart, S.R., 1993. Evidence for hotspot-related carbonatite metasomatism in the oceanic upper mantle. Nature 365, 221–227.

Hazen, R.M., Finger, L.W., 1979. Bulk modulus–volume relationship for cation–anion polyhedra. J. Geophys. Res. 84, 6723–6728.

Hill, E., Wood, B.J., Blundy, J.D., 2000. The effect of Ca-Tschermaks component on trace element partitioning between clinopyroxene and silicate melt. Lithos 53, 205–217.

Hirschmann, M.M., Ghiorso, M.S., 1994. Activities of nickel, cobalt, and manganese silicates in magmatic liquids and applications to olivine/liquid and to silicate/metal partitioning. Geochim. Cosmochim. Acta 58, 4109–4126.

Hofmann, A.W., 1988. Chemical differentiation of the earth: the relationship between mantle, continental crust, and oceanic crust. Earth Planet. Sci. Lett. 90, 297–314.

Janney, D.E., Banfield, J.F., 1998. Distribution of cations and vacancies and the structure of defects in oxidized intermediate olivine by atomic-resolution TEM and image simulation. Am. Mineral. 83, 799–810.

Jones, J.H., 1984. Temperature- and pressure-independent correlations of olivine/liquid partition coefficients and their application to trace element partitioning. Contrib. Mineral. Petrol. 88, 126–132.

Kelemen, P.B., Johnson, K.T.M., Kinzler, R.J., Irving, A.J., 1990. High-field-strength element depletions in arc basalts due to mantle–magma interaction. Nature 345, 521–524.

Kelemen, P.B., Shimizu, N., Dunn, T., 1993. Relative depletion of niobium in some arc magmas and the continental crust: partitioning of K, Nb, La and Ce during melt/rock reaction in the upper mantle. Earth Planet. Sci. Lett. 120, 111–134.

Kennedy, A.K., Lofgren, G.E., Wasserburg, G.J., 1993. An experimental study of trace element partitioning between olivine, orthopyroxene and melt in chondrules: equilibrium values and kinetic effects. Earth Planet. Sci. Lett. 115, 177–195.

Keppler, H., 1992. Crystal field spectra and geochemistry of transition metal ions in silicate melts and glasses. Am. Mineral. 77, 62–75.

Köhler, T.P., Brey, G.P., 1990. Calcium exchange between olivine and clinopyroxene calibrated as a geothermobarometer for natural peridotites from 2 to 60 kb with applications. Geochim. Cosmochim. Acta. 54, 2375–2388.

Kress, V.C., Carmichael, I.S.E., 1991. The compressibility of silicate liquids containing $Fe_2O_3$ and the effect of composition, temperature, oxygen fugacity and pressure on their redox state. Contrib. Mineral. Petrol. 108, 82–92.

Kudoh, Y., Takéuchi, Y., 1985. The crystal structure of forsterite $Mg_2SiO_4$ under high pressure up to 149 kb. Z. Kristallogr. 171, 291–302.

Le Maitre, R.W., Bateman, P., Dudek, A., Keller, J., Lameyre Le Bas, M.J., Sabiene, P.A., Schmid, R., Sorensen, H., Streckeisen, A., Woolley, A.R., Zanettin, B., 1989. A Classification of Igneous Rocks and Glossary of Terms. Blackwell, Oxford.

Libourel, G., 1999. Systematics of calcium partitioning between olivine and silicate melt: implications for melt structure and calcium content of magmatic olivines. Contrib. Mineral. Petrol. 136, 63–80.

McDade, P., Blundy, J.D., Wood, B.J., 2003. Trace element partitioning on the Tinaquillo lherzolite solidus at 1.5 GPa. Phys. Earth Planet. Int. 139, 129–147.

McKay, G.A., 1986. Crystal/liquid partitioning of REE in basaltic systems: extreme fractionation of REE in olivine. Geochim. Cosmochim. Acta 50, 69–79.

Nagasawa, H., 1966. Trace element partition coefficients in ionic crystals. Science 152, 767–769.

Oberti, R., Ungaretti, L., Cannillo, E., Hawthorne, F.C., 1992. The behaviour of Ti in amphiboles: $^{[4]}Ti^{4+}$ in richterite. Eur. J. Mineral. 4, 425–439.

Oberti, R., Vannucci, R., Zanetti, A., Tiepolo, M., Brumm, R., 2000. A crystal-chemical re-evaluation of amphibole/melt and amphibole/clinopyroxene $D_{Ti}$ in petrogenetic studies. Am. Mineral. 85, 401–419.

Ottolini, L., McDonough, W.F., 1996. Geochemistry of lithium and boron in the mantle: results from studies of peridotites. V.M. Goldschmidt Conference, March 31–April 4, Heidelberg (Germany). J. Conf. Abstr., vol. 1, p. 446.

Ottonello, G., Princivalle, F., Della Giusta, A., 1990. Temperature, composition, and $f_{O_2}$ effects on intersite distribution of Mg and $Fe^{2+}$ in olivines. Phys. Chem. Miner. 17, 301–312.

Ottolini, L., Bottazzi, P., Vannucci, R., 1993. Quantification of lithium, beryllium, and boron in silicates by secondary ion mass spectrometry using conventional energy filtering. Anal. Chem. 65, 1960–1968.

Purton, J.A., Allan, N.L., Blundy, J.D., 1997. Calculated solution energies of heterovalent cations in forsterite and diopside: implications for trace element partitioning. Geochim. Cosmochim. Acta 61, 3927–3936.

Purton, J.A., Blundy, J.D., Allan, N.L., 2000. Computer simulation of high-temperature, forsterite-melt partitioning. Am. Mineral. 85, 1087–1091.

Redfern, S.A.T., Artioli, G., Rinaldi, R., Henderson, C.M.B., Knight, K.S., Wood, B.J., 2000. Octahedral cation ordering in olivine at high temperature: II. An in situ powder diffraction study on synthetic $MgFeSiO_4$ (Fa50). Phys. Chem. Miner. 27, 630–637.

Rinaldi, R., Artioli, G., Wilson, C.C., McIntyre, G., 2000. Octahedral cation ordering in olivine at high temperature: I. In situ neutron single-crystal diffraction studies on natural mantle olivines (Fa12 and Fa10). Phys. Chem. Miner. 27, 623–629.

Robinson, J.A.C., Wood, B.J., Blundy, J.D., 1998. The beginning of melting of fertile and depleted peridotite at 1.5 GPa. Earth Planet. Sci. Lett. 155, 97–111.

Roeder, P.L., Emslie, R.F., 1970. Olivine–liquid equilibrium. Contrib. Mineral. Petrol. 29, 275–289.

Ryan, J.G., Langmuir, C.H., 1987. The systematics of lithium abundances in young volcanic rocks. Geochim. Cosmochim. Acta 51, 1727–1741.

Salters, V.J.M., Longhi, J.E., Bizimis, M., 2002. Near mantle solidus trace element partitioning at pressures up to 3.4 GPa. Geochem., Geophys., Geosyst., $G^3$. Paper number 2001GC000148.

Schiano, P., Clocchiatti, R., Joron, J.L., 1992. Melt and fluid inclusions in basalts and xenoliths from Tahaa Island, society archipelago: evidence for a metasomatised upper mantle. Earth Planet. Sci. Lett. 111, 69–82.

Shannon, R.D., 1976. Revised effective ionic radii in oxides and fluorides. Acta Cryst. A32, 751–757.

Skulski, T., Minarik, W., Watson, E.B., 1994. High-pressure experimental trace-element partitioning between clinopyroxene and basaltic melts. Chem. Geol. 117, 127–147.

Suzuki, T., Akaogi, M., 1995. Element partitioning between olivine and silicate melt under high pressure. Phys. Chem. Miner. 22, 411–418.

Taura, H., Yurimoto, H., Kurita, K., Sueno, S., 1998. Pressure dependence on partition coefficients for trace elements between olivine and coexisting melts. Phys. Chem. Miner. 25, 469–484.

Takahashi, E., 1978. Partitioning of $Ni^{2+}$, $Co^{2+}$, $Fe^{2+}$, $Mn^{2+}$ and $Mg^{2+}$ between olivine and silicate melts: compositional dependence of partition coefficient. Geochim. Cosmochim. Acta 42, 1829–1844.

Tiepolo, M., Vannucci, R., Oberti, R., Foley, S., Bottazzi, P., Zanetti, A., 2000a. Nb and Ta incorporation and fractionation in titanian pargasite and kaersutite. Crystal-chemistry constraints and implications for natural systems. Earth Planet. Sci. Lett. 76, 185–201.

Tiepolo, M., Vannucci, R., Oberti, R., Bottazzi, P., Zanetti, A., Foley, S. 2000b. Partitioning of rare earth elements, Y, Th, U, and Pb between pargasite, kaersutite, and basanite to trachyte melts: implications for percolated and veined mantle. Geochem., Geophys., Geosyst. $G^3$. Paper number No 2000GC000064.

Ulmer, P., 1989. The dependence of the $Fe^{2+}$–Mg cation-partitioning between olivine and basaltic liquid on pressure, temperature and composition. Contrib. Mineral. Petrol. 101, 261–273.

Urusov, V.D., 2001. The phenomenological theory of solid solution. In: Geiger, C.A. (Ed.), Solid Solutions in Silicate and Oxide Systems. EMU Notes in Mineralogy, vol. 3. Eötvös University Press, Budapest, pp. 121–151.

Van Westrenen, W., Allan, N.L., Blundy, J.D., Purton, J.A., Wood, B.J., 2000. Atomistic simulation of trace element incorporation into garnets—comparison with experimental garnet-melt partitioning data. Geochim. Cosmochim. Acta 64, 1629–1639.

Van Westrenen, W., Allan, N.L., Blundy, J.D., Lavrentiev, M.Yu., Lucas, B.R., Purton, J.A., 2003. Trace element incorporation into pyrope-grossular solid solutions: an atomistic simulation study. Phys. Chem. Miner. 30, 217–229.

Wood, B.J., Blundy, J.D., 1997. A predictive model for rare earth element partitioning between clinopyroxene and anhydrous silicate melt. Contrib. Mineral. Petrol. 129, 166–181.

Wood, B.J., Blundy, J.D., 2001. The effect of cation charge on crystal-melt partitioning of trace elements. Earth Planet. Sci Lett. 188, 59–71.

Worner, G., Viereck, L., Hertogen, J., Niephaus, H., 1989. The Mt Melbourne volcanic Field (Victoria Land, Antarctica): II. Geochemistry and magma genesis. Geol. Jahrb. E38, 395–433.

Xu, Y., Mercier, J.-C.C., Menzies, M.A., Ross, J.V., Harte, B., Lin, C., Shi, L., 1996. K-rich glass-bearing wehrlite xenoliths from Yitong, northeastern China: petrological and chemical evidence for mantle metasomatism. Contrib. Mineral. Petrol. 125, 406–420.